Development and Challenges of Large-Area All-Perovskite Tandem Solar Cells and Modules

Juncheng Wang, Jingwei Zhu, Cong Chen, Ulrich Wilhelm Paetzold, and Dewei Zhao**

The efficiency of all-perovskite tandem solar cells has recently surpassed that of single-junction perovskite solar cells, showing great potential as a future photovoltaic technology due to its low manufacturing cost and high power conversion efficiency potential, yet the size of these cells is still at the laboratory level. It is highly required to develop scalable preparation methods to fabricate large-area all-perovskite tandem solar modules for commercial applications. Herein, the key challenges encountered in the laboratory of all-perovskite tandem solar cells and the existing solutions are summarized and some views on the preparation of large areas and modules are given.

1. Introduction

Perovskite solar cells (PSCs) have been widely researched by researchers because of their excellent optical and electrical properties, including the tunable bandgaps, high absorption coefficient, long carrier lifetime, long carrier diffusion length, low exciton binding energy, and high defect tolerance.[1] The power conversion efficiency (PCE) of single-junction PSCs has rapidly increased from the initial 3.8% to certified 26.1%,[2] approaching the Shockley–Queisser (S–Q) limits, showing great competition in the future photovoltaic (PV) technology.[3] The S–Q limit of single-junction PSCs can be surpassed by constructing all-perovskite tandem solar cells (TSCs) consisting of a wide-bandgap (WBG; ≈1.75–1.8 eV) top subcell and a low-bandgap (LBG; ≈1.2–1.3 eV) bottom subcell.[4]

At present, a lot of impressive studies have reported on all-perovskite TSCs[5]; however, most of them have focused on small-area cells at the laboratory level or single-junction perovskite modules, and only very few works have reported progress on all-perovskite TSCs on large areas or modules. Improving the efficiency and stability of all-perovskite tandem solar modules (TSMs) by preparing uniform perovskite films with scalable preparation methods is currently the most challenging. Multiple reviews address the development of new and innovative passivation materials, charge-transport layers, improved perovskite compositions, and thin film morphologies. In this review, we revisit the development of all-perovskite TSCs with large areas as well as modules. Further, we discuss the challenges and future directions.

J. Wang, J. Zhu, C. Chen, D. Zhao
College of Materials Science and Engineering & Engineering Research Center of Alternative Energy Materials & Devices
Ministry of Education
Sichuan University
Chengdu 610065, China
E-mail: dewei.zhao@scu.edu.com

U. W. Paetzold
Institute of Microstructure Technology
Karlsruhe Institute of Technology
76344 Karlsruhe, Germany
E-mail: ulrich.paetzold@kit.edu

2. All-Perovskite TSCs

The performance of all-perovskite TSCs reflects on the performance of the WBG perovskite top subcell and LBG perovskite bottom subcell. In WBG PSCs, the nonradiative recombination losses are determined by halide phase segregation, interface defects, and energy level mismatch, which all lead to significant open-circuit voltage (V_{OC}) deficit and low fill factor (FF), which seriously affect the efficiency and stability.[6] For LBG PSCs, Sn^{2+} is easily oxidized to Sn^{4+}, forming a large number of Sn vacancies and inducing significant nonradiative recombination losses. Meanwhile, the excessive nucleation and crystallization rate during the film growth process will lead to uncontrollable morphology, increased film defects, and poor film quality.[7] So far, strategies have been proposed to improve the performance of all-perovskite TSCs: 1) optimize the compositions of WBG and LBG perovskite[8]; 2) incorporate the additives in the precursor solution to reduce the bulk defects of the perovskites[9]; 3) passivate the interface defects of perovskite films by post-treating the perovskite surface and selecting suitable charge-transport layers to reduce interfacial nonradiative recombination[10]; and 4) design and optimize the interconnecting layer (ICL) to reduce parasitic absorption and voltage losses, thereby increasing the overall short-circuit current density (J_{SC}) and V_{OC}.[11] In addition, these strategies also lead to more suitable energy-level matching and smoother charge transfer/transport, thus allowing higher FFs.[12]

In 2016, Zhou et al. reported the first two-terminal (2-T) all-perovskite TSC,[13] by using Spiro-OMeTAD/PEDOT:PSS/PEI/PCBM:PEI as the ICL. The resulting V_{OC} of the series solar cell reached 1.89 V, which is close to the sum of the two perovskite subcells. In the same year, Snaith et al. combined the WBG perovskite $FA_{0.83}Cs_{0.17}Pb(I_{0.5}Br_{0.5})_3$ (1.8 eV) as a top subcell with the tin (Sn)-lead (Pb) mixed LBG perovskite $FA_{0.75}Cs_{0.25}Sn_{0.5}Pb_{0.5}I_3$ (1.2 eV) as a bottom subcell to obtain a 2-T tandem cell with a PCE of 17.0%.[14] The use of indium tin oxide (ITO) as part of the ICL not only protects the layers

of the top subcell from the damage of the solution during the subsequent preparation of the bottom subcell, but also realizes the electrical coupling of the two subcells.

In 2018, Zhao and Yan et al. reported a bulk-passivation strategy via the incorporation of 2.5% chlorine, which increased the grain size of the Sn–Pb mixed LBG perovskite films, improved the crystallinity and carrier mobility, reduced the electron disorder, and inhibited the nonradiative recombination loss.[15] Based on this method, they successfully fabricated an efficient tin Sn–Pb mixed LBG PSC with a thick absorber layer (≈750 nm). Finally, on the basis of building Ag/MoO_x/ITO as ICL, the PCE of the 2-T all-perovskite TSCs was increased to ≈21%.

In 2019, Yan and Zhu et al. reduced the defect density of the films and improved the bulk quality by adding guanidine thiocyanate additives to the Sn–Pb mixed LBG precursor solution.[16] They obtained perovskite films with carrier lifetime greater than 1 µs and diffusion length greater than 2.5 µm, and finally 23.1%-efficiency 2-T all-perovskite TSCs. Subsequently, Tan et al. reduced the oxidized Sn^{4+} to Sn^{2+} by adding Sn powders to the Sn–Pb mixed LBG perovskite precursor in order to decrease the Sn vacancies.[17] The carrier diffusion length of the LBG perovskite films was increased to 3 µm. Moreover, they used atomic layer deposition (ALD)-prepared compact SnO_2 and thermally evaporated ultrathin gold (Au) layer (≈1 nm) to construct ICL, which not only effectively protects the WBG perovskite films, but also has low optical loss. A 24.8%-efficiency 2-T all-perovskite TSC was obtained.

In 2023, Zhao, Tang, and co-workers developed a new self-assembled monolayer (4-(7H-dibenzo[*c*,*g*]carbazol-7-yl butyl) phosphonic acid (4PADCB) by introducing two benzene rings into the carbazole of the commercial 4PACz material as the hole-transport layer (HTL) of WBG subcells in all-perovskite TSCs.[12a] The conjugated skeleton plane formed by two benzene rings at the end of the molecule can make 4PADCB have better charge transport ability than 4PACz, and its distorted spatial structure gives 4PADCB molecule good alcohol solubility and surface wettability, which is conducive to the preparation of large-area perovskite films without holes. 4PADCB can be more evenly anchored on ITO substrate, which is conducive to the uniform growth of WBG perovskite films on a large-area substrate, improves the hole extraction, and inhibits the nonradiative charge recombination at the buried interface. They achieved 1 cm^2 2-T all-perovskite tandems with a PCE of 27.0% (certified steady-state efficiency of 26.4%) and a V_{OC} of 2.12 V for an aperture area of 1.044 cm^2. Recently, Tan et al. developed a 3D/3D bilayer perovskite heterojunction (PHJ) at the Sn–Pb perovskite–electron-transport layer (ETL) interface to inhibit interface nonradiative recombination.[12b] They deposited an extremely thin layer of WBG perovskite on the surface of Sn–Pb mixed LBG perovskite film to form a bilayer PHJ to passivate interface defects and improve the PCE of LBG subcells. They achieved a high PCE of 28.5% (aperture area of 0.049 cm^2, certified 28.0% efficiency) of all-perovskite tandems, which is the highest efficiency reported for an all-perovskite TSC to date. And the PCE of the devices with an aperture area of 1.05 cm^2 reached 26.9%. These works have raised all-perovskite TSCs to ≈1 cm^2 levels, providing the basis for the preparation of larger area devices later.

3. All-Perovskite TSMs

From laboratory preparation to commercial production, the promotion of all-perovskite TSCs from small areas to large-area modules is essential. We summarize PCE advance of over 1 cm^2 large-area all-perovskite TSCs and modules in **Figure 1** and **Table 1**. At present, the method in focus for preparing high-quality perovskite films in the laboratory is spin coating; however, the spin coating technique is not suitable for fabricating large-area modules. This is mainly reflected by several points: 1) antisolvent is usually applied to control the crystallization of perovskite films during the spin coating process, which is difficult to control when preparing large areas; 2) the processing window of the spin coating is narrow, which is not suitable for the preparation process requiring a long drying time, and the fault tolerance rate is low in actual production; 3) during the spin coating process, most of the precursor ink is wasted, resulting in a waste of raw materials; 4) the linear velocity difference between the center region and the edge of the large substrate leads to poor film uniformity.[18] In addition, it is also difficult to deposit uniform and compact films on flexible large-area substrates by the spin coating method. Therefore, we need to choose more suitable expandable deposition methods as much as possible, including spray coating,[19] evaporation,[20] chemical vapor deposition,[21] blade coating,[22] and slot-die coating.[23] Among them, blade coating and slot-die coating have already been used to process large-area perovskite thin films for all-perovskite TSMs. In order to realize large-area module interconnection, the thin film stack is patterned in multiple monolithically connected cell stripes via the established P1, P2, and P3 laser scribes. The major challenge in realizing this module interconnection by layer patterning is the interplay or material removal during the ablation process and the arising material damage in the vicinity of the laser-scribed lines. Moreover, the area used for the monolithic interconnection, between P1 and P3, is a dead module area that needs to be minimized. To date the highest geometric FF (GFF) realized by laser patterning in all-perovskite TSMs is 96.1%,[24] which is close to the highest values reported for any thin-film PV technology.

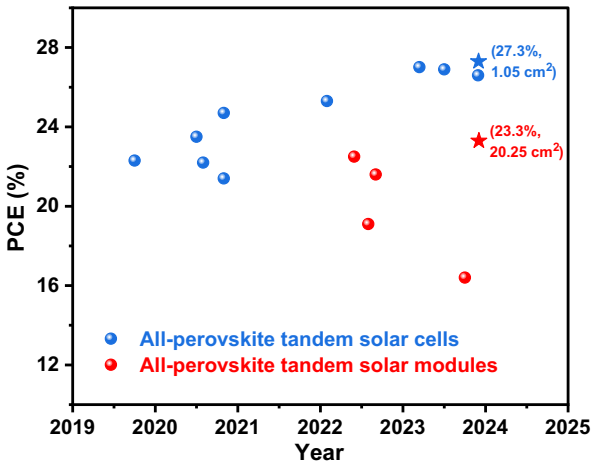

Figure 1. PCE development of over 1 cm^2 large-area all-perovskite TSCs and modules.

Table 1. Over 1 cm^2 large-area all-perovskite TSCs and modules.

Year	Device structure	Device type	Process	Area [cm^2]	PCE [%]	References
2019	ITO/PTAA/$FA_{0.8}Cs_{0.2}Pb(I_{0.6}Br_{0.4})_3$/$C_{60}$/ALD-$SnO_2$/Au/PEDOT:PSS/$FA_{0.7}MA_{0.3}Pb_{0.5}Sn_{0.5}I_3$/$C_{60}$/BCP/Cu	Cell	Spin coating	1.05	22.3	[17]
2020	ITO/NiO/VNPB/$FA_{0.8}Cs_{0.2}Pb(I_{0.6}Br_{0.4})_3$/$C_{60}$/ALD-$SnO_2$/Au/PEDOT:PSS/$FA_{0.7}MA_{0.3}Pb_{0.5}Sn_{0.5}I_3$/$C_{60}$/ALD-$SnO_2$/Cu	Cell	Spin coating	1.05	24.7	[29]
				12	21.4	
2020	ITO/PTAA/$Cs_{0.4}FA_{0.6}PbI_{1.95}Br_{1.05}$/$C_{60}$/$SnO_{2-x}$/$Cs_{0.05}MA_{0.45}FA_{0.5}Pb_{0.5}Sn_{0.5}I_3$/$C_{60}$/BCP/Cu	Cell	Spin coating	1.15	22.2	[30]
2021	ITO/NiO/VNPB/$FA_{0.8}Cs_{0.2}Pb(I_{0.62}Br_{0.38})_3$/$C_{60}$/ALD-$SnO_2$/Au/PEDOT:PSS/$FA_{0.7}MA_{0.3}Pb_{0.5}Sn_{0.5}I_3$/$C_{60}$/BCP/Cu	Cell	Spin coating	1.05	25.3	[31]
2022	IO:H/2PACz/$FA_{0.8}Cs_{0.2}(I_{0.6}Br_{0.4})_3$/LiF/$C_{60}$/$SnO_x$/ITO/PEDOT:PSS/$Cs_x(FA_{0.83}MA_{0.17})_{(1-x)}Sn_{0.5}Pb_{0.5}I_3$/PCBM/$C_{60}$/BCP/Cu	Module	Blade coating	12.25	19.1	[25]
2022	ITO/MB-NiO/2PACz and MeO-2PACz/$FA_{0.8}Cs_{0.2}PbI_{1.95}Br_{1.05}$/$C_{60}$/ALD-$SnO_2$/Au/PEDOT:PSS/$FA_{0.7}MA_{0.3}Pb_{0.5}Sn_{0.5}I_3$/$C_{60}$/BCP/Cu	Cell	Spin coating	1.05	23.5	[32]
2022	ITO/PTAA/$Cs_{0.25}FA_{0.75}Pb(I_{0.85}Br_{0.15})_3$/$C_{60}$/$SnO_2$/Au/PEDOT:PSS/$Cs_{0.2}FA_{0.8}Pb_{0.5}Sn_{0.5}I_3$/PCBM/$C_{60}$/BCP/Cu	Module	Blade coating	14.5	21.6	[26]
2023	ITO/NiO_x/VNPB/$Cs_{0.35}FA_{0.65}PbI_{1.8}Br_{1.2}$/$C_{60}$/ALD-$SnO_2$/Au/PEDOT:PSS/$FA_{0.7}MA_{0.3}Pb_{0.5}Sn_{0.5}I_3$/$C_{60}$/ALD-$SnO_2$/Ag	Module	Blade coating	20.25	22.5	[27]
2023	ITO/4PADCB/$FA_{0.8}Cs_{0.2}Pb(I_{0.6}Br_{0.4})_3$/$C_{60}$/ALD-$SnO_2$/IZO/PEDOT:PSS/$FA_{0.6}MA_{0.3}Cs_{0.1}Sn_{0.5}Pb_{0.5}I_3$/$C_{60}$/ALD-$SnO_2$/Cu	Cell	Spin coating	1.044	27.01	[12a]
2023	ITO/NiO/2PACz and MeO-2PACz/$FA_{0.8}Cs_{0.2}Pb(I_{0.62}Br_{0.38})_3$/$C_{60}$/ALD-$SnO_2$/Au/PEDOT:PSS/$FA_{0.7}MA_{0.3}Pb_{0.5}Sn_{0.5}I_3$/$C_{60}$/ALD-$SnO_2$/Cu	Cell	Spin coating	1.05	26.9	[12b]
2023	ITO/NiO_x/$Cs_{0.3}FA_{0.7}PbI_{1.8}Br_{1.2}$/$C_{60}$/$SnO_2$/Au/PEDOT:PSS/$FAPb_{0.5}Sn_{0.5}I_3$/$C_{60}$/BCP/Ag	Module	Blade coating	10.4	16.4	[22a]
2023	ITO/NiO_x/2PACz and MeO-2PACz/$FA_{0.8}Cs_{0.2}Pb(I_{0.62}Br_{0.38})_3$/$C_{60}$/ALD-$SnO_2$/ITO NCs/$FA_{0.7}MA_{0.3}Pb_{0.5}Sn_{0.5}I_3$/$C_{60}$/ALD-$SnO_2$/Cu	Cell	Spin coating	1.044	26.6	[33]
2023	ITO/NiO_x/2PACz and MeO-2PACz/$DMA_{0.1}Cs_{0.4}FA_{0.5}Pb(I_{0.72}Br_{0.24}Cl_{0.04})_3$/$C_{60}$/ALD-$SnO_2$/ITO NCs/$FAPb_{0.5}Sn_{0.5}I_3$/$C_{60}$/ALD-$SnO_2$/Cu	Cell	Spin coating	1.05	27.3	[34]
2023	ITO/NiO_x/2PACz and MeO-2PACz/$Cs_{0.35}FA_{0.65}PbI_{1.8}Br_{1.2}$/HF/ALD-$SnO_2$/Au/PEDOT:PSS/ $FA_{0.7}MA_{0.3}Pb_{0.5}Sn_{0.5}I_3$/HF/ALD-$SnO_2$/Cu	Module	Blade coating	20.25	23.3	[24]

In 2022, Paetzold and co-workers adopted a combination of blade coating and vacuum deposition to prepare a uniform large-area perovskite film and obtained a mini-module with all-perovskite tandem by laser scribing (**Figure 2**).[25] The module interconnection was realized by the established P1, P2, and P3 lines. The P1 line divides the front ITO into different cell stripes. Subsequently, the HTL, WBG perovskite layer, ETL if the WBG subcell, ICL, and the HTL, LBG perovskite layer, ETL in LBG subcell, were deposited using a variety of different scalable fabrication techniques. The P2 line serves to connect the ITO front electrode and the metal rear contact of two adjacent cell stripes. Finally, after depositing the top metal electrode, the P3 line is required to separate the different cell stripes at the rear contact (Figure 2a,b). They finally obtained a dead area enclosed between the P1 and P3 line obtaining a width of 210 μm, which corresponds to a GFF of up to 94.7%. To prevent the LBG precursor solution from resting for a long time on top of the underlying layers and to avoid degrade, the authors employed vacuum-assisted growth control (VAGC), which allows for a swift removal of solvents (Figure 2c). In addition to vacuum evacuation, they also moderated the gas flow by a small nitrogen flow unit, which resulted in a flow that further accelerated solvent extraction. They obtained a PCE of 19.1% (an aperture area of 12.25 cm^2) (Figure 2d,e).

Huang et al. proposed a hot gas-assisted blading method to prepare LBG perovskite films, which could accelerate the crystal growth process of perovskite, and the formed perovskite films were dense and thick (**Figure 3**a,b).[26] During blade coating deposition in the N_2 glove box, heated gas was uniformly blown to the surface of perovskite precursor film by air knife, and the temperature and flow rate of gas were precisely controlled to promote solvent volatilization to improve the crystal growth process of perovskite. With the assistance of hot gas, they quickly formed solid films with rapid solvent extraction, which avoided the use of antisolvent and was conducive to achieving high-speed scalable deposition. When N_2 was heated to 40, 70, and 100 °C, the crystal quality of perovskite films was obviously different (Figure 3d). At the same time, they reduced the DMSO/(Pb+Sn) molar ratio to 8% in perovskite films prepared with hot gas-assisted blades at 100 °C, forming a nonporous film with large single-crystal particles (Figure 3e). Then, they obtained monolithic all-perovskite TSMs with an efficiency of 21.6% (aperture area of 14.3 cm^2, GFF of 93.8%).

In the same year, Tan et al. reported that by fine-tuning the Cs content (denoted as x in the $Cs_xFA_{1-x}PbI_{1.8}Br_{1.2}$ formula) in WBG perovskites combined with a gas-assisted blade coating technique, the nucleation rate of crystals could be further controlled (**Figure 4**a).[27] When the content of Cs is 35%

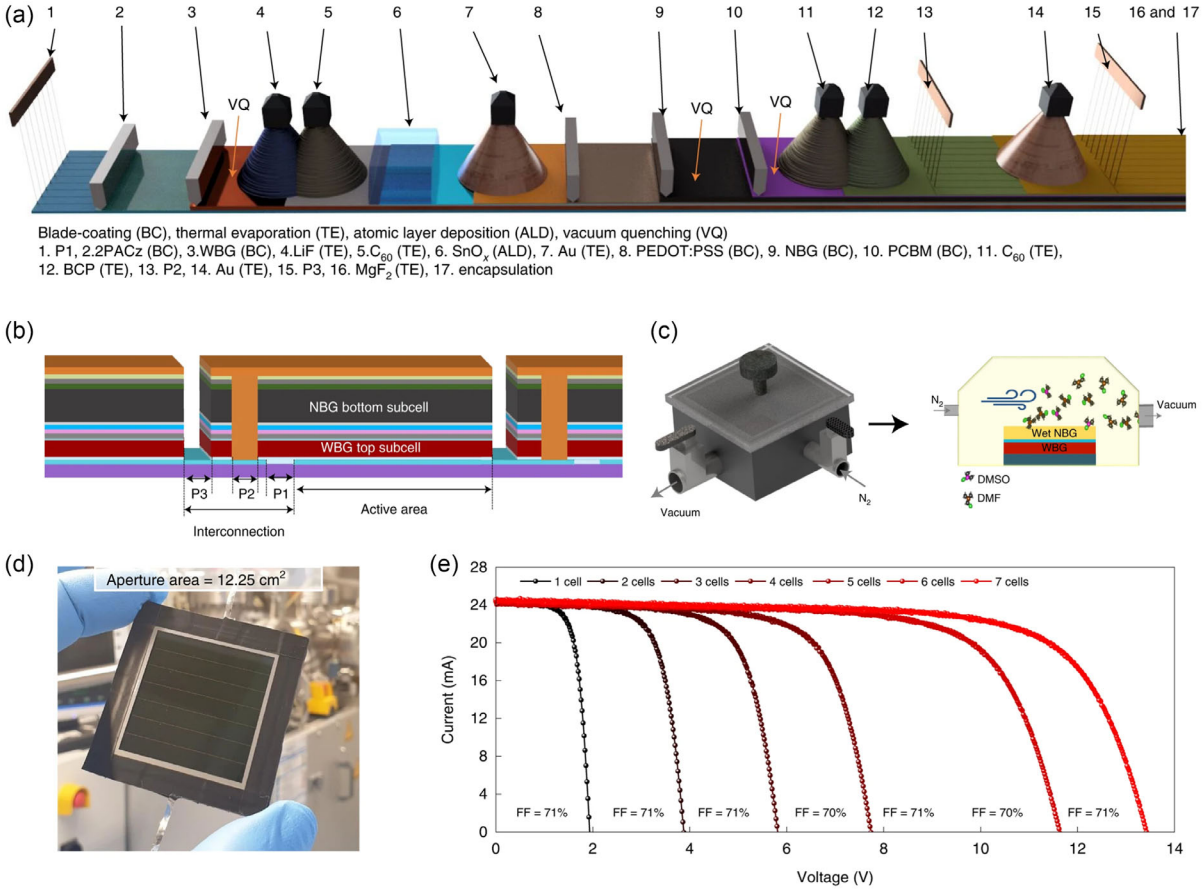

Figure 2. a) Schematic of the fabrication sequence for scalable processing of the tandem modules using a combination of blade coating and vacuum-deposition techniques. b) Schematic illustration of the 2-T all-perovskite TSM. c) Schematic of the designed vacuum plus nitrogen flowing chamber for growth of the LBG perovskite. d) The front side of the fabricated tandem module with seven cell strips and an aperture area of 12.25 cm^2. e) Current density–voltage (J–V) characteristic of stepwise accumulated tandem cell stripes of the module and the respective FFs. Reproduced with permission.[25] Copyright 2022, Springer Nature.

($Cs_{0.35}FA_{0.65}PbI_{1.8}Br_{1.2}$), the optimal WBG film quality is obtained (Figure 4b). It can be seen from the X-ray diffraction pattern that the $Cs_{0.35}FA_{0.65}PbI_{1.8}Br_{1.2}$ perovskite films exhibited the highest crystallinity (Figure 4c), and the devices had the best performance (Figure 4d). The photoluminescence quantum yield (PLQY) analysis of the combined device compared with the V_{OC} of WBG PSCs also showed that the nonradiative recombination loss could be effectively reduced by increasing the Cs content by $x = 0.35$ (Figure 4e). In addition, for all-perovskite TSCs, the ICL is usually a highly conductive transparent conductive oxide, and the contact between the last deposited metal electrode and ICL after marking the P2 may lead to a short circuit of the subcell. The metal electrode and perovskite diffused and reacted with each other, resulting in a decrease in efficiency and stability. They deposited about 10 nm thick ALD-SnO_2 after P2 scribing, which acted as a thin conformal diffusion barrier (CDB) to prevent the mutual diffusion and reaction between perovskite and metal electrode (Figure 4f). The champion tandem module exhibited a high PCE of 22.5% under reverse scan (certified PCE of 21.7%, GFF of 93.3%, aperture area of 20.25 cm^2), with a V_{OC} of 8.137 V, a J_{SC} of 3.60 mA cm^{-2}, and a FF of 76.8% (Figure 4g).

Thus far, only a few reports about all-perovskite TSMs have been reported, with the highest PCE being 23.3%.[24] In most of these reports, scalable blade coating technology has been used to obtain high-quality uniform films, assisted by an air knife or VAGC method. At the same time, the use of laser engraving can reduce the dead areas, which provides higher GFFs and thus improves the PCEs. These modules extend the areas of all perovskite TSCs gradually from the square centimeter scale to 20.25 cm^2, which opens the door to future commercialization.

4. Conclusion and Perspective

To date, only 2 years after the first reports, all-perovskite TSMs have achieved impressive PCE > 24.5% (aperture area of 20.25 cm^2); however, there is still large room for improvement compared to the record PCEs reported for small-area devices (29.1% efficiency @0.0489 cm^2).[2] All-perovskite TSMs face in

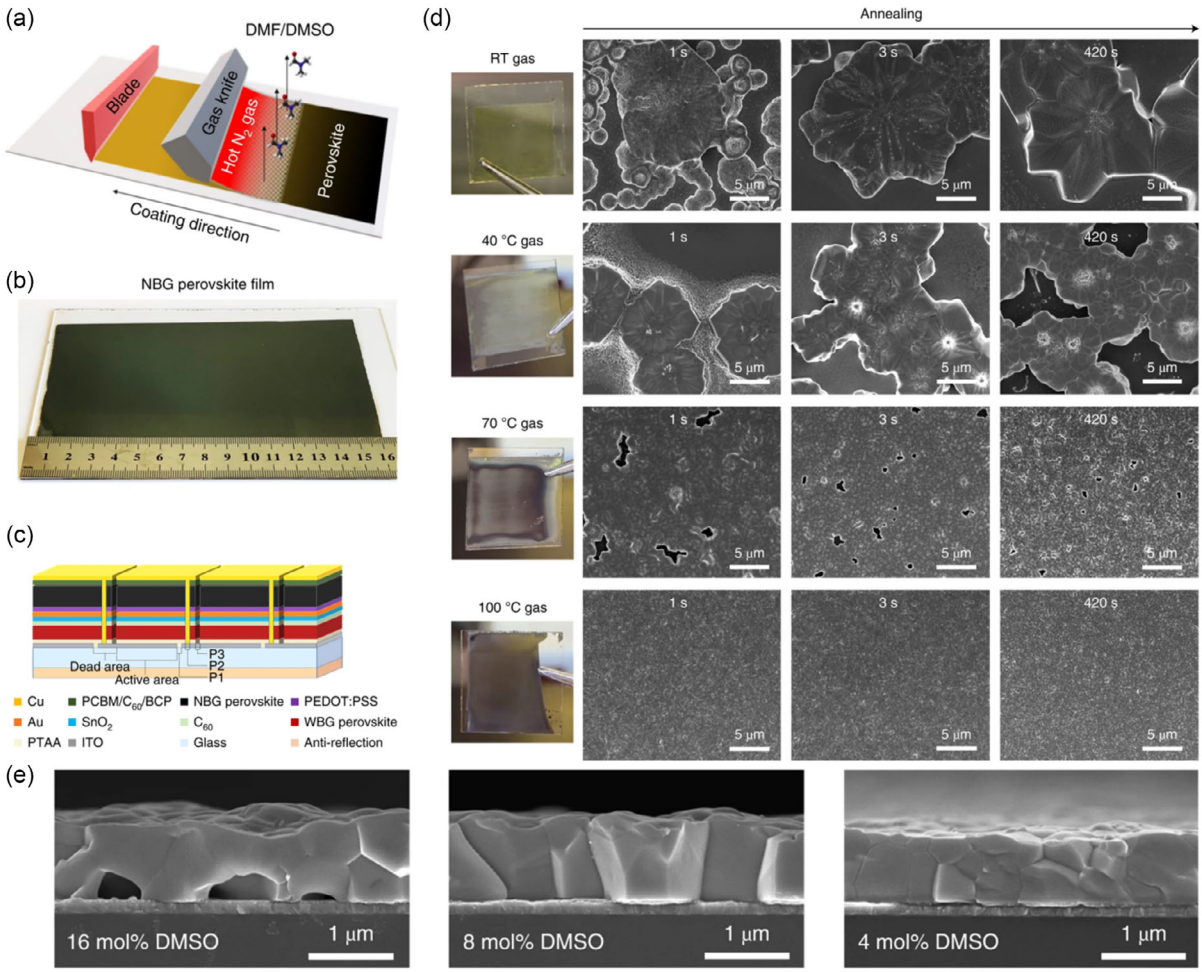

Figure 3. a) Schematic of hot gas-assisted blade coating. b) Picture of a blade-coated NBG perovskite film. c) Schematic structure of the all-perovskite tandem mini-module. d) Pictures and scanning electron microscopy (SEM) images of blade-coated LBG films with gas temperatures at room temperature, 40, 70, and 100 °C. e) Cross-sectional SEM images of blade-coated NBG films with 16, 8, and 4 mol% DMSO/(Sn+Pb) ratios in the precursor solution. Reproduced with permission.[26] Copyright 2022, Springer Nature.

many ways the same challenges as small-area all-perovskite TSCs, such as halide phase segregation in WBG PSCs, facile oxidation of Sn^{2+} in LBG PSCs, interface defects, energy-level mismatch, and energy losses at ICLs. Therefore, all-perovskite TSMs also need to consider the influence of different deposition methods on film quality. In order to close this gap in PCE and further improve the durability of all-perovskite TSMs, the following strategies are suggested[28]: 1) Exploiting the nucleation and growth processes and mechanisms of large-area films: Based on an improved understanding of these processes, it is expected that improved morphologies and homogeneity can be achieved for solution-processed perovskite thin films. Furthermore, gas- and vacuum-assisted deposition methods that are yet underrepresented in the development of all-perovskite TSMs bear the potential of controlled large-area thin film growth. 2) Developing approaches of high-quality large-area perovskite films: The optimization of chemical composition and the use of additives can further improve the quality of perovskite films, passivate defects, and reduce nonradiative recombination losses. For the preparation of uniform large-area perovskite films, the field shall explore more suitable components and additives to further control the film growth process, thereby improving the performance of the devices. 3) Designing and optimizing robust ICLs: A key challenge for all-perovskite TSCs is that the solubility of WBG perovskite in the top subcells is similar to that of LBG perovskite in the bottom subcells for solution-based fabrication methods. It is necessary to prepare a dense intermediate layer to protect WBG perovskite to avoid corrosion of the predeposited films. The ICLs should have a high transmittance in the near-infrared region to ensure sufficient absorption of LBG perovskites. Meanwhile, ICLs should also have good electrical conductivity to ensure smooth charge transport here. 4) Developing suitable and scalable charge transport materials: To reduce the nonradiative composite loss and parasitic absorption of light at the interface, due to the need for large-area preparation, the choice of charge transport materials should have a high infiltration of the perovskite precursor solution. 5) Optimizing laser scribing processes and developing advanced packaging

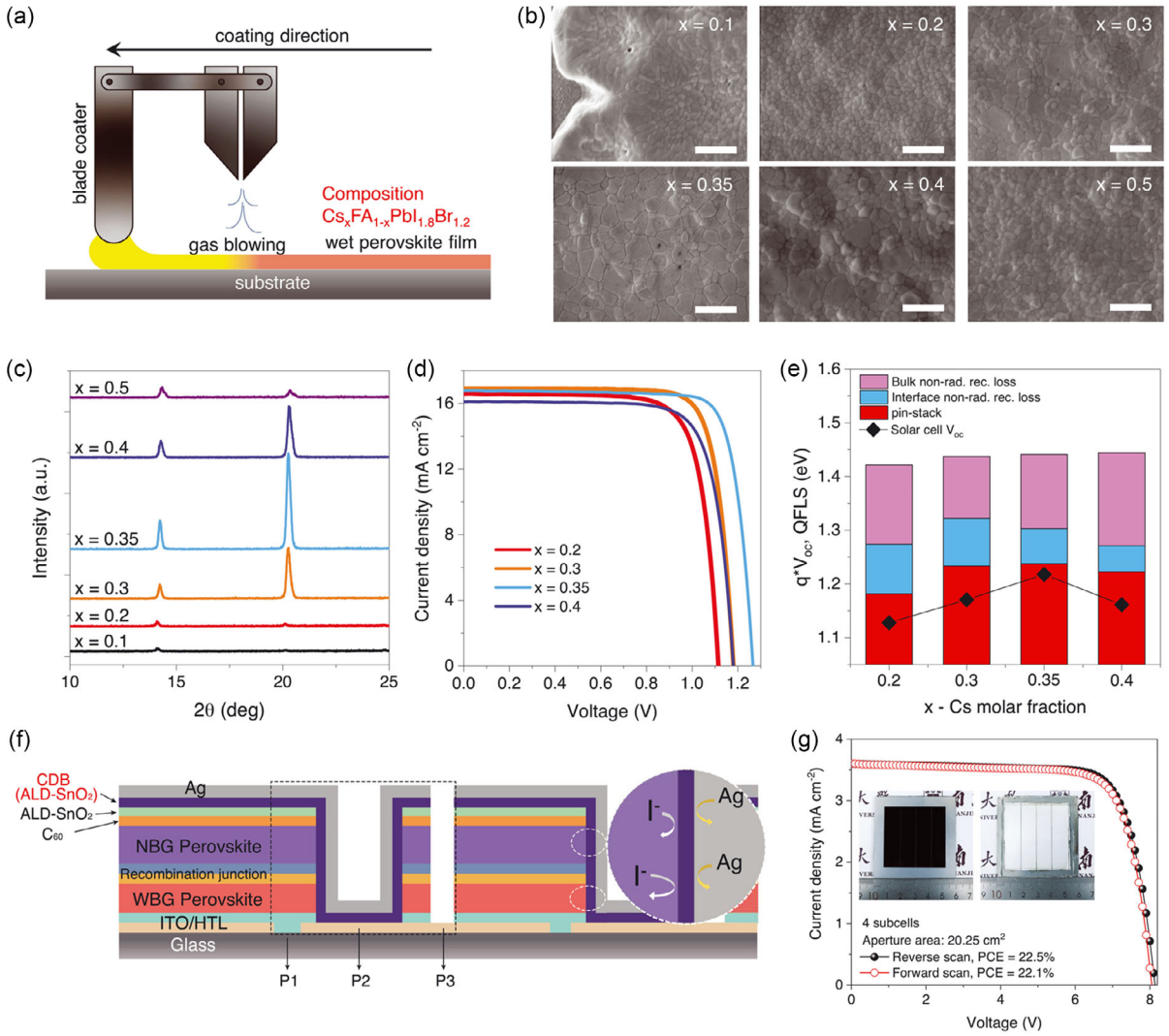

Figure 4. a) Schematic illustration of gas-assisted blade coating. b) SEM images of $Cs_xFA_{1-x}PbI_{1.8}Br_{1.2}$ perovskite films. c) X-ray diffraction pattern of $Cs_xFA_{1-x}PbI_{1.8}Br_{1.2}$ perovskite films. d) *J–V* curves of champion $Cs_xFA_{1-x}PbI_{1.8}Br_{1.2}$ PSCs. e) QFLS calculated from the PLQY for the respective perovskite films and the perovskites with transport layer stacks. f) Schematic diagram of the structure of the series-connected all-perovskite tandem module with CDB to prevent ion diffusion. g) *J–V* curves of the champion all-perovskite tandem module (aperture area of 20.25 cm^2, four subcells in series). Reproduced with permission.[27] Copyright 2022, American Association for the Advancement of Science.

techniques: High-throughput and high-precision laser can reduce the damage to perovskite film and reduce the dead area to improve the GFFs, and excellent packaging process can effectively avoid the degradation of perovskite film by water and oxygen in the environment to improve the stability of the device. Overall, continuous efforts and innovations will pave the way and make all-perovskite TSMs competitive with alternative PV technologies.

Acknowledgements

This work was financially supported by the National Key R&D Program of China (grant no. 2022YFB4200303), the National Natural Science Foundation of China (grant no. 62174112), the Fundamental Research Funds for the Central Universities (grant no. YJ2021157), and the Engineering Featured Team Fund of Sichuan University (grant no. 2020SCUNG102).

Conflict of Interest

The authors declare no conflict of interest.

Keywords

all-perovskite tandem solar cells, all-perovskite tandem solar modules, low-bandgap perovskites, wide-bandgap perovskites

[1] a) K. Wang, Z. Jin, L. Liang, H. Bian, D. Bai, H. Wang, J. Zhang, Q. Wang, S. Liu, *Nat. Commun.* **2018**, *9*, 4544; b) S. D. Stranks, G. E. Eperon, G. Grancini, C. Menelaou, M. J. P. Alcocer, T. Leijtens, L. M. Herz, A. Petrozza, H. J. Snaith, *Science* **2013**, *342*, 341; c) J. H. Noh, S. H. Im, J. H. Heo, T. N. Mandal, S. I. Seok, *Nano Lett.* **2013**, *13*, 1764; d) S. De Wolf, J. Holovsky, S.-J. Moon, P. Löper, B. Niesen, M. Ledinsky, F.-J. Haug, J.-H. Yum, C. Ballif, *J. Phys. Chem. Lett.* **2014**, *5*, 1035; e) J. Kang, L.-W. Wang, *J. Phys. Chem. Lett.* **2017**, *8*, 489.

[2] M. A. Green, E. D. Dunlop, M. Yoshita, N. Kopidakis, K. Bothe, G. Siefer, X. Hao, *Prog. Photovoltaics* **2023**, *32*, 3.

[3] W. Shockley, H. J. Queisser, *J. Appl. Phys.* **1961**, *32*, 510.

[4] J. Zhu, Y. Luo, R. He, C. Chen, Y. Wang, J. Luo, Z. Yi, J. Thiesbrummel, C. Wang, F. Lang, H. Lai, Y. Xu, J. Wang, Z. Zhang, W. Liang, G. Cui, S. Ren, X. Hao, H. Huang, Y. Wang, F. Yao, Q. Lin, L. Wu, J. Zhang, M. Stolterfoht, F. Fu, D. Zhao, *Nat. Energy* **2023**, *8*, 714.

[5] a) C. Li, Z. Song, C. Chen, C. Xiao, B. Subedi, S. P. Harvey, N. Shrestha, K. K. Subedi, L. Chen, D. Liu, Y. Li, Y.-W. Kim, C.-S. Jiang, M. J. Heben, D. Zhao, R. J. Ellingson, N. J. Podraza, M. Al-Jassim, Y. Yan, *Nat. Energy* **2020**, *5*, 768; b) C. Wang, Y. Zhao, T. Ma, Y. An, R. He, J. Zhu, C. Chen, S. Ren, F. Fu, D. Zhao, X. Li, *Nat. Energy* **2022**, *7*, 744; c) H. Chen, A. Maxwell, C. Li, S. Teale, B. Chen, T. Zhu, E. Ugur, G. Harrison, L. Grater, J. Wang, Z. Wang, L. Zeng, S. M. Park, L. Chen, P. Serles, R. A. Awni, B. Subedi, X. Zheng, C. Xiao, N. J. Podraza, T. Filleter, C. Liu, Y. Yang, J. M. Luther, S. De Wolf, M. G. Kanatzidis, Y. Yan, E. H. Sargent, *Nature* **2022**, *613*, 676; d) Z. Wang, L. Zeng, T. Zhu, H. Chen, B. Chen, D. J. Kubicki, A. Balvanz, C. Li, A. Maxwell, E. Ugur, R. dos Reis, M. Cheng, G. Yang, B. Subedi, D. Luo, J. Hu, J. Wang, S. Teale, S. Mahesh, S. Wang, S. Hu, E. D. Jung, M. Wei, S. M. Park, L. Grater, E. Aydin, Z. Song, N. J. Podraza, Z.-H. Lu, J. Huang, et al., *Nature* **2023**, *618*, 74; e) S. Zhou, S. Fu, C. Wang, W. Meng, J. Zhou, Y. Zou, Q. Lin, L. Huang, W. Zhang, G. Zeng, D. Pu, H. Guan, C. Wang, K. Dong, H. Cui, S. Wang, T. Wang, G. Fang, W. Ke, *Nature* **2023**, *624*, 69.

[6] a) C. Chen, J. Liang, J. Zhang, X. Liu, X. Yin, H. Cui, H. Wang, C. Wang, Z. Li, J. Gong, Q. Lin, W. Ke, C. Tao, B. Da, Z. Ding, X. Xiao, G. Fang, *Nano Energy* **2021**, *90*, 106608; b) R. He, Z. Yi, Y. Luo, J. Luo, Q. Wei, H. Lai, H. Huang, B. Zou, G. Cui, W. Wang, C. Xiao, S. Ren, C. Chen, C. Wang, G. Xing, F. Fu, D. Zhao, *Adv. Sci.* **2022**, *9*, 2203210.

[7] a) Q. Chen, J. Luo, R. He, H. Lai, S. Ren, Y. Jiang, Z. Wan, W. Wang, X. Hao, Y. Wang, J. Zhang, I. Constantinou, C. Wang, L. Wu, F. Fu, D. Zhao, *Adv. Energy Mater.* **2021**, *11*, 2101045; b) S. J. Lee, S. S. Shin, J. Im, T. K. Ahn, J. H. Noh, N. J. Jeon, S. I. Seok, J. Seo, *ACS Energy Lett.* **2017**, *3*, 46.

[8] a) Q. Jiang, J. Tong, R. A. Scheidt, X. Wang, A. E. Louks, Y. Xian, R. Tirawat, A. F. Palmstrom, M. P. Hautzinger, S. P. Harvey, S. Johnston, L. T. Schelhas, B. W. Larson, E. L. Warren, M. C. Beard, J. J. Berry, Y. Yan, K. Zhu, *Science* **2022**, *378*, 1295; b) P. Wu, J. Wen, Y. Wang, Z. Liu, R. Lin, H. Li, H. Luo, H. Tan, *Adv. Energy Mater.* **2022**, *12*, 2202948.

[9] a) Y. Zhao, C. Wang, T. Ma, L. Zhou, Z. Wu, H. Wang, C. Chen, Z. Yu, W. Sun, A. Wang, H. Huang, B. Zou, D. Zhao, X. Li, *Energy Environ. Sci.* **2023**, *16*, 2080; b) J. Luo, R. He, H. Lai, C. Chen, J. Zhu, Y. Xu, F. Yao, T. Ma, Y. Luo, Z. Yi, Y. Jiang, Z. Gao, J. Wang, W. Wang, H. Huang, Y. Wang, S. Ren, Q. Lin, C. Wang, F. Fu, D. Zhao, *Adv. Mater.* **2023**, *35*, 2300352.

[10] a) S. Hu, K. Otsuka, R. Murdey, T. Nakamura, M. A. Truong, T. Yamada, T. Handa, K. Matsuda, K. Nakano, A. Sato, K. Marumoto, K. Tajima, Y. Kanemitsu, A. Wakamiya, *Energy Environ. Sci.* **2022**, *15*, 2096; b) W. Wang, X. Liu, J. Wang, C. Chen, J. Yu, D. Zhao, W. Tang, *Adv. Energy Mater.* **2023**, *13*, 2300694.

[11] X. Zhou, H. Lai, T. Huang, C. Chen, Z. Xu, Y. Yang, S. Wu, X. Xiao, L. Chen, C. J. Brabec, Y. Mai, F. Guo, *ACS Energy Lett.* **2022**, *8*, 502.

[12] a) R. He, W. Wang, Z. Yi, F. Lang, C. Chen, J. Luo, J. Zhu, J. Thiesbrummel, S. Shah, K. Wei, Y. Luo, C. Wang, H. Lai, H. Huang, J. Zhou, B. Zou, X. Yin, S. Ren, X. Hao, L. Wu, J. Zhang, J. Zhang, M. Stolterfoht, F. Fu, W. Tang, D. Zhao, *Nature* **2023**, *618*, 80; b) R. Lin, Y. Wang, Q. Lu, B. Tang, J. Li, H. Gao, Y. Gao, H. Li, C. Ding, J. Wen, P. Wu, C. Liu, S. Zhao, K. Xiao, Z. Liu, C. Ma, Y. Deng, L. Li, F. Fan, H. Tan, *Nature* **2023**, *620*, 994.

[13] F. Jiang, T. Liu, B. Luo, J. Tong, F. Qin, S. Xiong, Z. Li, Y. Zhou, *J. Mater. Chem. A* **2016**, *4*, 1208.

[14] G. E. Eperon, T. Leijtens, K. A. Bush, R. Prasanna, T. Green, J. T.-W. Wang, D. P. McMeekin, G. Volonakis, R. L. Milot, R. May, A. Palmstrom, D. J. Slotcavage, R. A. Belisle, J. B. Patel, E. S. Parrott, R. J. Sutton, W. Ma, F. Moghadam, B. Conings, A. Babayigit, H.-G. Boyen, S. Bent, F. Giustino, L. M. Herz, M. B. Johnston, M. D. McGehee, H. J. Snaith, *Science* **2016**, *354*, 861.

[15] D. Zhao, C. Chen, C. Wang, M. M. Junda, Z. Song, C. R. Grice, Y. Yu, C. Li, B. Subedi, N. J. Podraza, X. Zhao, G. Fang, R.-G. Xiong, K. Zhu, Y. Yan, *Nat. Energy* **2018**, *3*, 1093.

[16] J. Tong, Z. Song, D. H. Kim, X. Chen, C. Chen, A. F. Palmstrom, P. F. Ndione, M. O. Reese, S. P. Dunfield, O. G. Reid, J. Liu, F. Zhang, S. P. Harvey, Z. Li, S. T. Christensen, G. Teeter, D. Zhao, M. M. Al-Jassim, M. F. A. M. van Hest, M. C. Beard, S. E. Shaheen, J. J. Berry, Y. Yan, K. Zhu, *Science* **2019**, *364*, 475.

[17] R. Lin, K. Xiao, Z. Qin, Q. Han, C. Zhang, M. Wei, M. I. Saidaminov, Y. Gao, J. Xu, M. Xiao, A. Li, J. Zhu, E. H. Sargent, H. Tan, *Nat. Energy* **2019**, *4*, 864.

[18] Y. Cheng, Y. Peng, A. K. Y. Jen, H.-L. Yip, *Sol. RRL* **2021**, *6*, 2100545.

[19] a) N. Rolston, W. J. Scheideler, A. C. Flick, J. P. Chen, H. Elmaraghi, A. Sleugh, O. Zhao, M. Woodhouse, R. H. Dauskardt, *Joule* **2020**, *4*, 2675; b) J. E. Bishop, J. A. Smith, C. Greenland, V. Kumar, N. Vaenas, O. S. Game, T. J. Routledge, M. Wong-Stringer, C. Rodenburg, D. G. Lidzey, *ACS Appl. Mater. Interfaces* **2018**, *10*, 39428.

[20] a) J. Li, H. Wang, X. Y. Chin, H. A. Dewi, K. Vergeer, T. W. Goh, J. W. M. Lim, J. H. Lew, K. P. Loh, C. Soci, T. C. Sum, H. J. Bolink, N. Mathews, S. Mhaisalkar, A. Bruno, *Joule* **2020**, *4*, 1035; b) J. Li, H. A. Dewi, H. Wang, J. H. Lew, N. Mathews, S. Mhaisalkar, A. Bruno, *Sol. RRL* **2020**, *4*, 2000473.

[21] a) G. Tong, J. Zhang, T. Bu, L. K. Ono, C. Zhang, Y. Liu, C. Ding, T. Wu, S. Mariotti, S. Kazaoui, Y. Qi, *Adv. Energy Mater.* **2023**, *13*, 2300153; b) Z. Liu, L. Qiu, E. J. Juarez-Perez, Z. Hawash, T. Kim, Y. Jiang, Z. Wu, S. R. Raga, L. K. Ono, S. Liu, Y. Qi, *Nat. Commun.* **2018**, *9*, 3880.

[22] a) Y. Shi, J. Sun, J. Zhou, T. Wen, C. Zou, D. Liu, F. Liu, S. Yang, Y. Deng, Z. Yang, *Adv. Funct. Mater.* **2023**, 2307209; b) Y. Deng, C. H. Van Brackle, X. Dai, J. Zhao, B. Chen, J. Huang, *Sci. Adv.* **2019**, *5*, eaax7537; c) L. Zeng, Z. Chen, S. Qiu, J. Hu, C. Li, X. Liu, G. Liang, C. J. Brabec, Y. Mai, F. Guo, *Nano Energy* **2019**, *66*, 104099.

[23] a) Z. Yang, W. Zhang, S. Wu, H. Zhu, Z. Liu, Z. Liu, Z. Jiang, R. Chen, J. Zhou, Q. Lu, Z. Xiao, L. Shi, H. Chen, L. K. Ono, S. Zhang, Y. Zhang, Y. Qi, L. Han, W. Chen, *Sci. Adv.* **2021**, *7*, eabg3749; b) M. Xu, W. Ji, Y. Sheng, Y. Wu, H. Cheng, J. Meng, Z. Yan, J. Xu, A. Mei, Y. Hu, Y. Rong, H. Han, *Nano Energy* **2020**, *74*, 104842.

[24] H. Sun, K. Xiao, H. Gao, C. Duan, S. Zhao, J. Wen, Y. Wang, R. Lin, X. Zheng, H. Luo, C. Liu, P. Wu, W. Kong, Z. Liu, L. Li, H. Tan, *Adv. Mater.* **2023**, *36*, 2308706.
[25] B. Abdollahi Nejand, D. B. Ritzer, H. Hu, F. Schackmar, S. Moghadamzadeh, T. Feeney, R. Singh, F. Laufer, R. Schmager, R. Azmi, M. Kaiser, T. Abzieher, S. Gharibzadeh, E. Ahlswede, U. Lemmer, B. S. Richards, U. W. Paetzold, *Nat. Energy* **2022**, *7*, 620.
[26] X. Dai, S. Chen, H. Jiao, L. Zhao, K. Wang, Z. Ni, Z. Yu, B. Chen, Y. Gao, J. Huang, *Nat. Energy* **2022**, *7*, 923.
[27] K. Xiao, Y.-H. Lin, M. Zhang, R. D. J. Oliver, X. Wang, Z. Liu, X. Luo, J. Li, D. Lai, H. Luo, R. Lin, J. Xu, Y. Hou, H. J. Snaith, H. Tan, *Science* **2022**, *376*, 762.
[28] a) J. M. C. da Silva Filho, A. D. Gonçalves, F. C. Marques, J. N. de Freitas, *Sol. RRL* **2021**, *6*, 2100865; b) J. Zhu, D. Zhao, *Innovation* **2023**, *4*, 100493.
[29] K. Xiao, R. Lin, Q. Han, Y. Hou, Z. Qin, H. T. Nguyen, J. Wen, M. Wei, V. Yeddu, M. I. Saidaminov, Y. Gao, X. Luo, Y. Wang, H. Gao, C. Zhang, J. Xu, J. Zhu, E. H. Sargent, H. Tan, *Nat. Energy* **2020**, *5*, 870.
[30] Z. Yu, Z. Yang, Z. Ni, Y. Shao, B. Chen, Y. Lin, H. Wei, Z. J. Yu, Z. Holman, J. Huang, *Nat. Energy* **2020**, *5*, 657.
[31] R. Lin, J. Xu, M. Wei, Y. Wang, Z. Qin, Z. Liu, J. Wu, K. Xiao, B. Chen, S. M. Park, G. Chen, H. R. Atapattu, K. R. Graham, J. Xu, J. Zhu, L. Li, C. Zhang, E. H. Sargent, H. Tan, *Nature* **2022**, *603*, 73.
[32] L. Li, Y. Wang, X. Wang, R. Lin, X. Luo, Z. Liu, K. Zhou, S. Xiong, Q. Bao, G. Chen, Y. Tian, Y. Deng, K. Xiao, J. Wu, M. I. Saidaminov, H. Lin, C.-Q. Ma, Z. Zhao, Y. Wu, L. Zhang, H. Tan, *Nat. Energy* **2022**, *7*, 708.
[33] C. Liu, R. Lin, Y. Wang, H. Gao, P. Wu, H. Luo, X. Zheng, B. Tang, Z. Huang, H. Sun, S. Zhao, Y. Guo, J. Wen, F. Fan, H. Tan, *Angew. Chem., Int. Ed.* **2023**, *62*, 202313374.
[34] J. Wen, Y. Zhao, P. Wu, Y. Liu, X. Zheng, R. Lin, S. Wan, K. Li, H. Luo, Y. Tian, L. Li, H. Tan, *Nat. Commun.* **2023**, *14*, 7118.